Research Article

Elham Kamgar, Hanna Maria Baranowska, Massoud Kaykhaii, Marcin Nowicki*, Przemysław Łukasz Kowalczewski and Joanna Zembrzuska*

Assessment of molecular dynamics in natural Shilajit using low-field NMR relaxometry for geographical traceability

https://doi.org/10.1515/revac-2025-0097
Received May 14, 2025; accepted December 16, 2025; published online January 19, 2026

Abstract: Shilajit (Mumijo) is a phytomineral exudate known for its therapeutic potential, traditionally used in Ayurvedic medicine. Its molecular composition and consequently its therapeutic properties are influenced by geographical origin. Low-field nuclear magnetic resonance (LF NMR) offers a non-destructive tool to assess the molecular behavior of Shilajit rapidly and non-destructively. Twelve raw Shilajit samples from five regions (Iran, India, Nepal, Russia, and Kyrgyzstan) were analyzed using LF NMR at 15 MHz. Longitudinal magnetization relaxation (T_1) and transverse magnetization relaxation (T_2) relaxation times were measured using an inversion-recovery and Carr–Purcell–Meiboom–Gill pulse sequence, respectively. Three distinct relaxation behavior groups were identified. Group I showed only T_1 (solid samples with undetectable T_2), group II exhibited single T_1 and T_2 (moderately viscous, hydrated samples), while group III revealed biphasic T_2 relaxation (indicating proton heterogeneity). Clear differences in relaxation profiles were observed across geographical origins, with Iranian samples showing the widest range of T_1 values, while Russian and some Iranian samples exhibited dual T_2 components. LF NMR relaxation parameters (T_1, T_2) are strongly dependent on the geographic origin and molecular structure of Shilajit. The technique shows promise for use in authentication and traceability of Shilajit, enabling differentiation based on relaxation signatures.

Keywords: Shilajit; low-field NMR relaxometry; health supplements; phytomineral; geographic traceability; authentication

***Corresponding authors: Marcin Nowicki**, Department of Entomology and Plant Pathology, University of Tennessee, Knoxville, TN 37996, USA, E-mail: mnowicki@utk.edu. https://orcid.org/0000-0002-2655-5464; and **Joanna Zembrzuska**, Department of General and Analytical Chemistry, Institute of Chemistry and Technical Electrochemistry, Faculty of Chemical Technology, Poznan University of Technology, Poznań, Poland, E-mail: joanna.zembrzuska@put.poznan.pl. https://orcid.org/0000-0002-3993-4818

Elham Kamgar, Department of General and Analytical Chemistry, Institute of Chemistry and Technical Electrochemistry, Faculty of Chemical Technology, Poznan University of Technology, Poznań, Poland, E-mail: elham.kamgar@doctorate.put.poznan.pl. https://orcid.org/0000-0003-3729-8499

Hanna Maria Baranowska, Department of Physics and Biophysics, Faculty of Food Science and Nutrition, Poznań University of Life Sciences, Poznań, Poland, E-mail: hanna.baranowska@up.poznan.pl. https://orcid.org/0000-0001-6597-0858

Massoud Kaykhaii, Department of Analytical Chemistry, Faculty of Natural Sciences, Comenius University Bratislava, Bratislava, Slovakia, E-mail: massoud.kaykhaii@uniba.sk. https://orcid.org/0000-0003-2890-9286

Przemysław Łukasz Kowalczewski, Faculty of Health Sciences, Andrzej Frycz Modrzewski Krakow University, Kraków, Poland, E-mail: pkowalczewski@uafm.edu.pl. https://orcid.org/0000-0002-0153-4624

1 Introduction

Shilajit (Mumijo) is a natural phytomineral exudate that oozes from sedimentary rocks in high-altitude mountain ranges, most notably in the Himalayas mountain range (1,000–5,000 m), as well as in other countries such as the Iran, Russia, Pakistan, and Afghanistan. Its formation is attributed to the prolonged microbial decomposition of plant material under specific geological and environmental conditions over centuries, resulting in a complex mixture rich in bioactive compounds [1–3]. The chemical composition of Shilajit is predominantly humic substances (60–80%), particularly fulvic acid (15–20%), inorganic anions, alongside dibenzo-α-pyrones, triterpenes, sterols, fatty acids, phenolic lipids, amino acids, trace elements such as thallium and arsenic, and major cations such as calcium and magnesium [1, 2, 4, 5]. Fulvic acid, a major constituent, has been shown to possess strong antioxidant, anti-inflammatory, and immunomodulatory properties [5]. It facilitates the transport of minerals and nutrients across cell membranes and is

Open Access. © 2026 the author(s), published by De Gruyter. This work is licensed under the Creative Commons Attribution 4.0 International License.

considered a key driver of Shilajit's bioactivity [2, 6]. The dibenzo-α-pyrones and their chromoprotein conjugates are thought to be critical in enhancing mitochondrial function, supporting energy metabolism, and improving endurance, making Shilajit a notable adaptogen [4, 7, 8]. Recent comparative studies using advanced analytical techniques such as GC–MS/MS, LC, and ICP-OES confirmed that regional deposits (e.g., India, Pakistan, Iran, Nepal, and Russia) differ in their phytochemical and elemental profiles, underlining the importance of provenance for both quality control and therapeutic potential [3, 5, 9].

Ayurvedic medicine is a traditional system of medicine that originated in India more than 3,000 years ago based on a holistic approach integrating diet, lifestyle, herbal remedies, and body–mind practices to maintain or restore health. From a scientific perspective, it combines empirically derived treatments with philosophical concepts such as the balance of doshas (biological energies), though many of its principles and therapies remain under investigation for clinical efficacy and safety [10–12]. Traditionally used in Ayurvedic medicine under the category of *Rasayana* (rejuvenators), Shilajit is described as a "destroyer of weakness" and "conqueror of mountains," suggesting its role in enhancing strength, vitality, and overall health [1]. Contemporary studies have corroborated these claims, demonstrating that Shilajit supplementation (at doses of 250–500 mg/day) is associated with improved testosterone levels, enhanced sperm quality, better cognitive performance, and protection against oxidative stress and inflammation [2, 8]. Moreover, in preclinical studies, it has shown promise in neuroprotection, especially in the context of Alzheimer's disease, due to its ability to inhibit tau protein aggregation and reduce neuroinflammation [13–15]. Despite its long-standing use, the pharmacokinetics and mechanisms of action of many Shilajit constituents remain under investigation. Nevertheless, growing evidence supports its integration into evidence-based phytotherapy for metabolic, reproductive, and neurodegenerative conditions, warranting further mechanistic and clinical research.

Low-field nuclear magnetic resonance (LF NMR) is a non-destructive and non-invasive spectroscopic technique that enables the analysis of interactions between protons, primarily those originating from water or lipids. Of particular interest are its capabilities for determining the mode of water binding within biological matrices – such as plant or animal tissues – as well as its application in studying micelle formation in emulsion systems [16, 17]. The nuclear relaxation process within a spin system involves the dissipation of energy accumulated as a result of exposure to an oscillating magnetic field. Transverse relaxation is associated with energy transfer between neighboring nuclear spins. The time required for the system to return to thermodynamic equilibrium is referred to as the spin–spin relaxation time, denoted as T_2. In contrast, the transfer of energy to the surrounding lattice, commonly termed the "spin–lattice" system, occurs over a longer duration and is characterized by the longitudinal magnetization relaxation time, designated as T_1 [18]. The restoration of thermodynamic equilibrium at the molecular level is influenced by the local magnetic and electric environments surrounding the excited atomic nuclei. The values of both T_1 and T_2 are governed by spin interactions arising from molecular dynamics of proton-containing compounds [19]. In liquids, a decrease in T_1 is typically observed with increasing viscosity. In some cases, T_1 reaches a minimum value, beyond which a further increase in viscosity leads to an elongation of T_1 [20]. Transitions between energy states are induced by fluctuations of the local magnetic field, which are, in turn, caused by the motion of molecules and magnetically active particles [21, 22]. An increase in molecular ordering among proton-containing species accelerates the rate of relaxation transitions at the microscopic level. This phenomenon manifests as a reduction in T_1 values. Concurrently, the maximum amplitude of local magnetic field fluctuations shifts toward lower frequencies. When the fluctuation frequency falls below the resonance frequency, the efficiency of longitudinal magnetization relaxation is reduced, leading to an increase in T_1 [23, 24]. The transverse magnetization relaxation time (T_2) exhibits a monotonic decline from high values – typical of low-viscosity liquids – to low values characteristic of solids with rigid, highly ordered structures [25, 26]. The transfer of energy absorbed from the electromagnetic pulse occurs as a spin at a higher energy level transfers energy to another spin at a lower energy state, a process defined as transverse magnetization relaxation. As the molecular system becomes more ordered, the T_2 relaxation time decreases accordingly.

Considering the above, this study aimed to investigate whether significant variations exist in the LF NMR relaxation properties of Shilajit samples originating from diverse geographical regions. The specific objective was to determine if the relaxation parameters (T_1 and T_2) can serve as reliable molecular fingerprints reflecting differences in chemical composition, viscosity, hydration state, and structural ordering of the samples. By systematically comparing materials obtained from Iran, India, Nepal, Russia, and Kyrgyzstan, we sought to establish whether LF NMR relaxometry can not only capture the inherent physicochemical heterogeneity of Shilajit but also provide a non-destructive analytical basis for its authentication and geographical traceability. In this way, the study addresses both a fundamental question – how regional origin shapes the molecular dynamics of this

complex phytomineral – and a practical need for tools supporting quality control and provenance verification in nutraceutical and pharmaceutical applications.

2 Materials and methods

2.1 Samples origin

This study utilized twelve raw Shilajit samples, designated S1–S12 (Figure 1). Their geographical origins were as follows: Iran (S1 – unknown region, S2 – Lorestan, S4 – Kurdistan, S5 – Ravar, S6 – Bijar, S9 – Kahnuj, S11 – Saravan), India (S7 – unknown region, S12 – Himalaya), Nepal (S3 – unknown region), Russia (S8 – unknown region), and Kyrgyzstan (S10 – unknown region). Figure 2 presents the appearance of the selected samples.

2.2 Relaxometry

The experimental investigations were conducted using a pulsed nuclear magnetic resonance (NMR) spectrometer (Ellab, Poznań, Poland) operating at a resonance frequency of 15 MHz. T_1 were determined using the inversion-recovery pulse sequence (180–TI–90–TR) [18]. All measurements were performed at a temperature of 20.0 ± 0.5 °C. Depending on the spin density, between 4 and 8 signal accumulations were employed. The volume of the samples analyzed during the measurements ranged from 0.08 to 0.15 cm^3. Due to the heterogeneity of the samples, individual adjustment of measurement sequences was required. In each case, the durations of the 180° and 90° radiofrequency pulses were optimized accordingly. The interpulse delays (T_1) were selected for each sample based on the analysis of the free induction decay (FID) signal crossing zero amplitude, with the aid of a predefined variable table. The repetition time (TR) for the inversion-recovery sequence was selected in accordance with the respective T_1 relaxation times. Samples characterized by relatively high proton density – evidenced by FID signals of high amplitude – were analyzed with five signal accumulations. In contrast, samples exhibiting lower spin density yielded FID signals with smaller amplitudes, necessitating an increase in the number of accumulations to ten. The Marquardt minimization method was utilized to fit the multi-exponential decays. The accuracy of the relaxation

Figure 1: Origin of the analyzed samples.

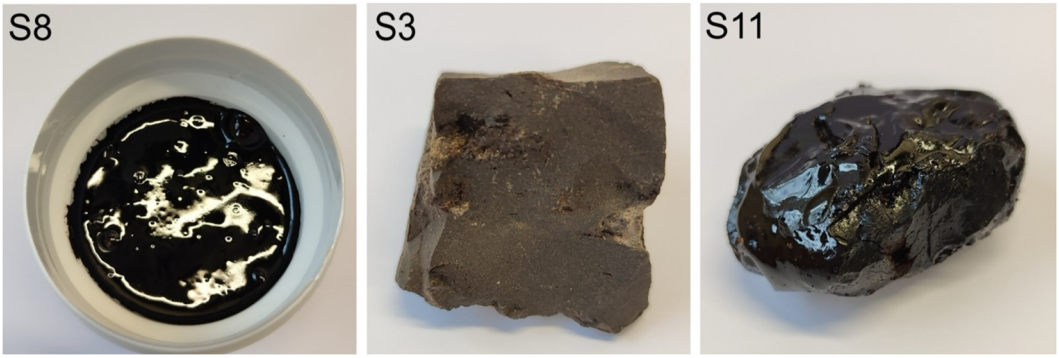

Figure 2: Representative photographs of selected Shilajit samples, demonstrating the variability in structural characteristics among the analyzed materials.

parameters was determined, and standard deviations were calculated. The temporal changes in the current amplitude of the FID signal at the applied pulse frequency were described by Eq. (1):

$$M_z(t) = M_0\left(1 - 2e^{\frac{-t}{T_1}}\right) \quad (1)$$

where $M_z(t)$ is the actual magnetization value, M_0 is the equilibrium magnetization value, t is the delay between pulses, and T_1 is the relaxation time.

Depending on the type of material analyzed, appropriate interpulse delays (t) between radiofrequency pulses were applied. For each measurement, 32 FID signals were collected. Between 4 and 10 signal accumulations were performed, depending on the sample type.

To determine T_2, the Carr–Purcell–Meiboom–Gill (CPMG) pulse sequence (90–TE/2–$(180)_n$–TR) [27, 28] was used. As in the T_1 measurements, each sample required individual optimization of the pulse sequence parameters. The spin echo train was generated only for samples in which the T_2 relaxation times were sufficiently long to allow reliable measurement. The T_2 time values involved an adjustment of values of the echo amplitudes to Eq. (2):

$$M_{x,y}(\mathrm{TE}) = M_0 \sum_{i=1}^{n} p_i e^{\frac{-\mathrm{TE}}{T_{2i}}} \quad (2)$$

where $M_{x,y}$ (TE) is the echo amplitude, M_0 is the equilibrium amplitude, TE is the distance between π impulses, and p_i is the fraction of protons relaxing with the T_{2i} transverse magnetization relaxation time.

For the analyzed samples, 50–100 spin-echo signals were acquired. The echo time (TE) was individually adjusted for each sample within the range of 0.002–0.150 ms, with 10 signal accumulations performed in all measurements.

The T_1 relaxation times were calculated using the CracSpin software package [29], while T_2 values were derived by fitting the decay of the spin echo amplitudes to single- or double-exponential models using the TableCurve software, with the application of the least squares method.

2.3 Statistical analyses

All measurements were repeated in triplicate, unless otherwise stated. Statistica 13 software (Dell Software Inc., Round Rock, TX, USA) was used to perform a one-way analysis of variance (ANOVA). A post-hoc Tukey HSD (honestly significant difference) multiple comparison test was used to identify statistically homogeneous subsets at $\alpha = 0.05$.

3 Results and discussion

Twelve samples originating from diverse geographical locations were analyzed using LF NMR spectroscopy. The results, summarized in Table 1, indicate the presence of three distinct groups based on relaxation behavior: (1) samples characterized solely by a T_1, namely, samples S2, S3, S5, S7, S9, and S11; (2) samples described by one T_1 and one T_2 relaxation time, including S4, S6, S10, and S12; and (3) samples exhibiting one T_1 and two distinct T_2 relaxation times, represented by S1 and S8.

In systems where proton-containing molecules are bound to the matrix in different ways, distinct proton fractions can be observed, each relaxing with different and distinguishable spin–spin relaxation times. Under such conditions, a biexponential decay of spin echo amplitudes is detected. The shorter relaxation times (T_{21}) correspond to the *short component* of the spin–spin relaxation process and are associated with protons belonging to less mobile species, which are more strongly bound to the matrix. In contrast, the longer relaxation times (T_{22}) represent the *long component* and correspond to the relaxation of protons from more mobile molecular species [30, 31].

Table 1: Values of T_1 and T_2 relaxation times of Shilajit samples from various geographical origins, including short T_{21} and long T_{22} transverse magnetization relaxation times, with corresponding fraction of protons relaxing (p).

Sample	T_1 [ms]	T_2 [ms]	T_{21} [ms]	T_{22} [ms]	p
S1	5.519 ± 0.399^{e}		0.015 ± 0.002^{b}	0.937 ± 0.076^{a}	0.30^{b}
S2	41.335 ± 6.480^{b}	nd*			
S3	0.424 ± 0.032^{h}	nd			
S4	30.352 ± 1.225^{c}	0.125 ± 0.010^{c}			
S5	21.728 ± 3.007^{d}	nd			
S6	24.073 ± 0.193^{cd}	19.018 ± 3.225^{a}			
S7	30.865 ± 6.332^{c}	nd			
S8	2.000 ± 0.092^{f}		0.231 ± 0.012^{a}	0.784 ± 0.045^{b}	0.68^{a}
S9	68.371 ± 1.925^{a}	nd			
S10	0.730 ± 0.066^{g}	0.143 ± 0.02^{c}			
S11	16.554 ± 3.528^{d}	nd			
S12	23.450 ± 0.163^{cd}	2.467 ± 0.057^{b}			

*nd, not detected. Values marked with the same superscript letter do not differ significantly $p > 0.05$.

The first group of samples consists of solid-state systems with an ordered structure (Figure 3). This is evidenced by the extremely short T_2 relaxation time, which is undetectable using the employed measurement system. In these experiments, the smaller the T_1 value, the more relaxed the macroscopic structure becomes. A reduction in T_1 could be a result of decreased structural ordering, which may translate to an increase in viscosity. However, another factor contributing to changes in T_1 could be components of the samples that are rich in paramagnetic ions. The presence of such ions significantly shortens relaxation times even in systems with relatively low viscosity coefficients [32].

The second group of analyzed samples (Figure 4) is characterized by a single T_1 and a single T_2. This group exhibits significant variation in the values of both relaxation times. The cause of this variation is attributable to both the chemical composition of the samples and the ordering of their structure. Sample S6, described by relaxation times with similar values, is a liquid sample with a relatively low viscosity coefficient. However, it contains several large hydrophilic molecules, compared to the water molecule. Water molecules form a hydration shell around these hydrophilic molecules. The shorter relaxation times, compared to pure water, result from the significant binding of water to the hydrophilic surfaces [33–35]. Similar results were obtained for sample S10. However, the notably lower values of both T_1 and T_2 indicate the presence of substances that shorten relaxation times, in conjunction with large hydrophilic molecules. Both factors work additively to reduce the relaxation times in liquid systems [36–38]. Samples S4 and S12 exhibit similar T_1 values but significantly different T_2 values. This suggests different structural ordering in these

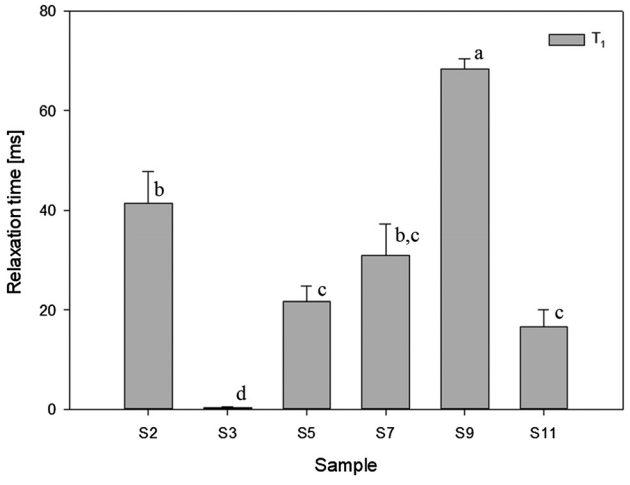

Figure 3: Results of longitudinal magnetization relaxation time (T_1).

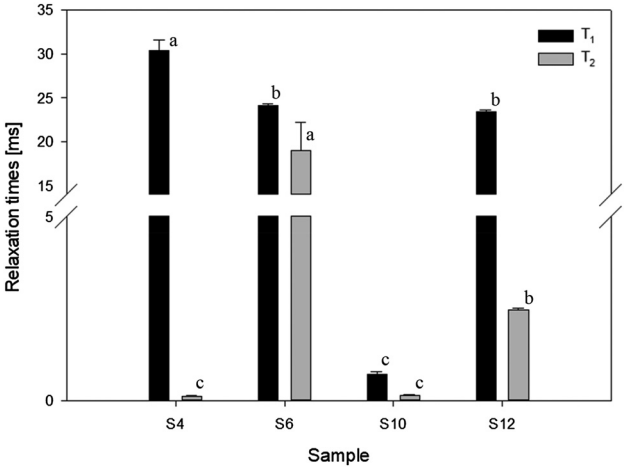

Figure 4: Results of longitudinal magnetization relaxation time and transverse magnetization relaxation time.

samples. Sample S12, compared to S4, is considerably less viscous. The similar chemical composition of both samples, in terms of paramagnetic ion presence, is evidenced by the comparable T_1 values [39, 40]. The differing T_2 values suggest distinct macroscopic structures that lead to differences in viscosity coefficients.

The third group of the analyzed samples was characterized by two T_2 relaxation times (Figure 5). This result indicates that in the studied systems, protons exist in two distinct fractions due to their molecular dynamics. Similar findings are observed in biological systems, such as muscles or emulsions [41, 42]. The lower T_1 value (sample S8 compared to sample S1) suggests more significant interactions between proton-containing particles and large macromolecules. This is confirmed by the higher value of T_{21} and the larger fraction of protons relaxing with this time (the short component in this system). The above observations are consistent with the results for sample S1, where a smaller fraction of protons with shorter T_2 times is observed, alongside a longer relaxation time for the second proton fraction. Sample S1 contains significantly fewer hydrophilic macromolecules compared to sample S8. It should be emphasized that the presence of two proton fractions may also be associated with the presence of lipids in quantities large enough to cause the separation of signals originating from protons, for example, in water molecules and protons present in fatty acid chains [43, 44].

The description of the groups of research material samples can be analyzed based on their geographical origin. The relaxation times with the highest values are characterized by samples from Iran (S9, S2, S4, S7, S6, S12, S5), with values ranging from 68 to 21 ms. Among these, however, samples S4, S6, and S12 (from Iran, Kurdistan, and India) are additionally described by individual values of T_2 relaxation times. Therefore, it can be inferred that they constitute a subgroup with distinct molecular motion properties of protons. The biological matrix is characteristic of systems exhibiting quasi-plastic-like properties. Similar properties, albeit with significantly limited particle movement of proton-containing substances, are exhibited by sample S10 from Kyrgyzstan. The results obtained from the analysis using LF NMR suggest that samples S4, S6, S12, and additionally sample S10 contain significant amounts of fats, which are critical from the perspective of molecular properties of protons [45]. Thus, the presence of a group of protons with relatively long T_2 relaxation times will determine the viscoelastic mechanical properties, dominated by viscous characteristics [32, 46].

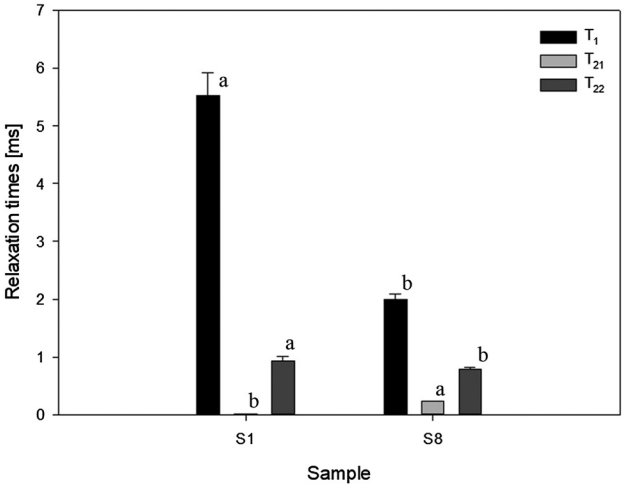

Figure 5: Results of longitudinal magnetization relaxation time and two components of transverse magnetization relaxation times.

The T_1 and T_2 relaxation times obtained from low-field NMR measurements revealed clear distinctions in the relaxation profiles of Shilajit samples depending on their geographical origin. Among Iranian samples, a wide range of T_1 values was observed – from as low as 0.424 ms (S3 – region unknown) to as high as 68.371 ms (S9 – Kahnuj). This variability suggests significant microstructural and molecular differences among deposits from different Iranian regions. Notably, sample S9 exhibited the highest T_1 value across all tested samples, indicative of a higher proportion of mobile proton fractions, possibly associated with reduced viscosity or a looser molecular matrix [47, 48]. Furthermore, Iranian samples displayed inconsistent T_2 profiles. Only S4 (Kurdistan) and S6 (Bijar) yielded measurable T_2 relaxation values, with S6 presenting a notably high T_2 value (19.018 ms), in contrast to the much lower T_2 of S4 (0.125 ms). The remaining Iranian samples (S2, S5, S9, and S11) lacked detectable T_2 components, suggesting a condensed and rigid organic matrix with low levels of mobile protons [49, 50].

In contrast, samples of non-Iranian origin exhibited more consistent relaxation behaviors. The Himalayan sample from India (S12) showed a moderate T_1 (23.450 ms) and a relatively long T_2 (2.467 ms), indicative of a well-hydrated moderately viscous matrix. Of particular interest were samples S1 (Iran, unknown region) and S8 (Russia), both displaying biphasic T_2 components. Sample S1 demonstrated an extremely short T_{21} (0.015 ms) alongside a longer T_{22} (0.937 ms), while S8 exhibited higher T_{21} (0.231 ms) and slightly shorter T_{22} (0.784 ms). The presence of dual T_2 relaxation components suggests molecular heterogeneity, possibly reflecting the coexistence of tightly bound protons (e.g., within colloidal phases) and more mobile fractions (e.g., loosely bound water or micellar structures). Remarkably low T_1 values were recorded for the Nepalese (S3, 0.424 ms) and Kyrgyz (S10, 0.730 ms) samples, implying either high molecular ordering or elevated viscosity. In both cases,

the absence (S3) or presence of only a short T_2 (S10, 0.143 ms) supports the hypothesis of a densely packed, highly structured organic phase, potentially rich in humic or polyphenolic complexes.

4 Conclusions

This study demonstrates that the LF NMR relaxometry, as an effective non-destructive method, can differentiate between Shilajit samples based on their geographical origin, offering a potential marker of regional provenance. Key differentiating features include high T_1 values (>40 ms): indicative of southeastern Iranian origin (e.g., S2 and S9); very low T_1 values (<1 ms): characteristic of Nepalese and Kyrgyz samples (S3 and S10), and the presence of dual T_2 components: observed in samples from Russia and some regions of Iran (S1 and S8). These findings show that LF NMR relaxometry can be applied as a reliable tool for the authentication and geographical traceability of Shilajit, contributing to quality control measures in the food and nutraceutical industries. Future research should focus on expanding the sample set to include a broader range of geographical sources and processing conditions, as well as integrating LF NMR data with complementary analytical techniques to enhance the robustness of Shilajit authentication protocols.

Funding information: Authors state no funding involved.
Author contribution: All authors have accepted responsibility for the entire content of this manuscript and consented to its submission to the journal, reviewed all the results and approved the final version of the manuscript. EK – investigation, data curation, formal analysis, writing (original draft/review & editing); HMB – methodology, investigation, conceptualization; MK – formal analysis; MN – writing (original draft/review & editing); PŁK – conceptualization, writing (original draft/review & editing); JZ – supervision, writing (original draft/review & editing).
Conflict of interest: Authors state no conflict of interest.
Data availability statement: The datasets generated during and/or analyzed during the current study are available from the corresponding author (J.Z.) on reasonable request.

References

1. Bhavsar SK, Thaker AM, Malik JK. Shilajit. In: Nutraceuticals: efficacy, safety and toxicity. London, UK: Elsevier; 2016:707–16 pp.
2. Garedew A, Feist M, Schmolz E, Lamprecht I. Thermal analysis of mumiyo, the legendary folk remedy from the Himalaya region. Thermochim Acta 2004;417:301–9.
3. Kamgar E, Kaykhaii M, Zembrzuska J. A comprehensive review on Shilajit: what we know about its chemical composition. Crit Rev Anal Chem 2023;55:1–13.
4. Das A, El Masry MS, Gnyawali SC, Ghatak S, Singh K, Stewart R, et al. Skin transcriptome of middle-aged women supplemented with natural herbo-mineral shilajit shows induction of microvascular and extracellular matrix mechanisms. J Am Coll Nutr 2019;38:526–36.
5. Kamgar E, Zembrzuska J, Lorenc W, Kaykhaii M. Screening and quantification of inorganic anions in Shilajit and its supplements. BMC Chem 2025;19:95.
6. Perumal P, Sathakkathulla NA, Kumaran K, Ravikumar R, Selvaraj JJ, Nagendran V, et al. Green synthesis of zinc oxide nanoparticles using aqueous extract of shilajit and their anticancer activity against HeLa cells. Sci Rep 2024;14:2204.
7. Das A, Datta S, Rhea B, Sinha M, Veeraragavan M, Gordillo G, et al. The human skeletal muscle transcriptome in response to oral shilajit supplementation. J Med Food 2016;19:701–9.
8. Pandit S, Biswas S, Jana U, De RK, Mukhopadhyay SC, Biswas TK. Clinical evaluation of purified Shilajit on testosterone levels in healthy volunteers. Andrologia 2016;48:570–5.
9. Kamgar E, Zembrzuska J, Zembrzuski W, Kaykhaii M. Quantifying of thallium in Shilajit and its supplements to unveil the potential risk of consumption of this popular traditional medicine. BMC Chem 2025; 19:20.
10. Chattopadhyay K, Wang H, Kaur J, Nalbant G, Almaqhawi A, Kundakci B, et al. Effectiveness and safety of ayurvedic medicines in type 2 diabetes mellitus management: a systematic review and meta-analysis. Front Pharmacol 2022;13:821810.
11. Narayana DBA, Durg S. Ayurveda: where is the evidence. J Ayurveda Integr Med 2021;12:408–11.
12. Patwardhan B. Bridging Ayurveda with evidence-based scientific approaches in medicine. EPMA J 2014;5:19.
13. Carrasco-Gallardo C, Guzmán L, Maccioni RB. Shilajit: a natural phytocomplex with potential procognitive activity. Int J Alzheimers Dis 2012;2012:1–4.
14. Frolova LN, Kiseleva TL. Chemical composition of mumijo and methods for determining its authenticity and quality (a review). Pharm Chem J 1996;30:543–7.
15. Kaźmierkiewicz K, Chojnacka M, Lis ME, Ciechańska E, Kapuśniak K, Suszczyńska W, et al. The effect of fulvic acid on Alzheimer's disease – a systematic review. Quality in Sport 2025;41:60196.
16. Gašparová M, Tokárová Z. Low-field nuclear magnetic resonance as an environmentally benign and energy saving analytical tool in organic laboratories. Int J Environ Sci Technol 2025;22:8691–703.
17. Wang X-Y, Xie J, Chen X-J. Applications of non-invasive and novel methods of low-field nuclear magnetic resonance and magnetic resonance imaging in aquatic products. Front Nutr 2021;8:651804.
18. Brosio E, Gianferri R. Low-resolution NMR—An analytical tool in food characterization. In: Brosio E, editor. Basic NMR in food characterization. Kerala, India: Research Signpost; 2009:9–37 pp.
19. Calero C, Martí J, Guàrdia E. ^{1}H nuclear spin relaxation of liquid water from molecular dynamics simulations. J Phys Chem B 2015;119:1966–73.
20. Lewandowicz J, Ostrowska-Ligeza E, Baranowska HM. Gelatinization of starch: a comparative study of viscographic, differential scanning calorimetry and low field NMR analyses. In: Rapkova R, Copikova J, editors. 16th international conference on polysaccharides-glycoscience. Czech Chemical Society; 2020:9–14 pp.
21. Bothner-By AA. Magnetic field induced alignment of molecules. In: Encyclopedia of magnetic resonance. Prague, Czech Republic: John Wiley & Sons, Ltd; 2007.

22. Chaddah P. Magnetic field induced 1st order transitions: recent studies, and some new concepts. AIP Conf Proc 2015;1661:030002.
23. Baranowska HM. Water molecular properties in forcemeats and finely ground sausages containing plant fat. Food Biophys 2011;6: 133–7.
24. Jeżowski P, Menzel J, Baranowska HM, Kowalczewski PŁ. Microwaved-assisted synthesis of starch-based biopolymer membranes for novel green electrochemical energy storage devices. Materials 2023;16:7111.
25. Kowalczewski PŁ, Walkowiak K, Masewicz Ł, Smarzyński K, Thanh-Blicharz JL, Kačániová M, et al. LF NMR spectroscopy analysis of water dynamics and texture of gluten-free bread with cricket powder during storage. Food Sci Technol Int 2021;27: 776–85.
26. Nishiyama Y, Hou G, Agarwal V, Su Y, Ramamoorthy A. Ultrafast magic angle spinning solid-state NMR spectroscopy: advances in methodology and applications. Chem Rev 2023;123:918–88.
27. Carr HY, Purcell EM. Effects of diffusion on free precession in nuclear magnetic resonance experiments. Phys Rev 1954;94:630–8.
28. Meiboom S, Gill D. Modified spin-echo method for measuring nuclear relaxation times. Rev Sci Instrum 1958;29:688–91.
29. Weglarz WP, Haranczyk H. Two-dimensional analysis of the nuclear relaxation function in the time domain: the program CracSpin. J Phys Appl Phys 2000;33:1909–20.
30. Blümich B. Introduction to compact NMR: a review of methods. TrAC, Trends Anal Chem 2016;83:2–11.
31. Tang F, Vasas M, Hatzakis E, Spyros A. Magnetic resonance applications in food analysis. Annu Rep NMR Spectrosc 2019;98:239–306.
32. Alexandre J, Feio G, Marvão MR, Figueiredo J. Correlation between high power proton T_2 NMR relaxation and macroscopic viscoelastic properties. Mater Sci Forum 2004;455–456:459–62.
33. D'Amico F, Bencivenga F, Camisasca G, Gessini A, Principi E, Cucini R, et al. Thermodynamic hydration shell behavior of glycine. J Chem Phys 2013;139:015101.
34. Zhang J, Liu L, Chen Y, Wang B, Ouyang C, Tian Z, et al. Water dynamics in the hydration shell of amphiphilic macromolecules. J Phys Chem B 2019;123:2971–7.
35. Zhang J, Yan Y, Wang B, Liu L, Li S, Tian Z, et al. Water dynamics in the hydration shell of hyper-branched poly-ethylenimine. Phys Chem Chem Phys 2022;24:18393–400.
36. D'Agostino C, Bräuer P, Charoen-Rajapark P, Crouch MD, Gladden LF. Effect of paramagnetic species on T_1, T_2 and T_1/T_2 NMR relaxation times of liquids in porous $CuSO_4/Al_2O_3$. RSC Adv 2017;7:36163–7.
37. Payne KM, Wilds JM, Carniato F, Botta M, Woods M. On water and its effect on the performance of T_1-Shortening contrast agents. Isr J Chem 2017;57:880–6.
38. Richardson PM, Voice AM, Ward IM. NMR T_1 relaxation time measurements and calculations with translational and rotational components for liquid electrolytes containing $LiBF_4$ and propylene carbonate. J Chem Phys 2013;139:214501.
39. Cioran AM, Teixidor F, Viñas C. The effect of a paramagnetic metal ion within a molecule: comparison of the structurally identical paramagnetic $[3,3\text{-Fe}(1,2\text{-}C_2B_9H_{11})_2]^-$ with the diamagnetic $[3,3\text{-Co}(1,2\text{-}C_2B_9H_{11})_2]^-$ sandwich complexes. Dalton Trans 2015;44:2809–18.
40. Kolbanev IV, Degtyarev EN, Streletskii AN, Kokorin AI. Paramagnetic centers created under mechanochemical treatment of mixed molybdenum-vanadium oxides. Appl Magn Reson 2016;47:575–88.
41. Han S. Characterization of biological systems via relaxometric and diffusimetric NMR. SSRN Electron J 1998. https://doi.org/10.2139/ssrn.1944911.
42. Saab G, Thompson RT, Marsh GD, Picot PA, Moran GR. Two-dimensional time correlation relaxometry of skeletal muscle *in vivo* at 3 tesla. Magn Reson Med 2001;46:1093–8.
43. Alexandri E, Ahmed R, Siddiqui H, Choudhary M, Tsiafoulis C, Gerothanassis I. High resolution NMR spectroscopy as a structural and analytical tool for unsaturated lipids in solution. Molecules 2017;22:1663.
44. Watts A. Solid-state NMR approaches for studying the interaction of peptides and proteins with membranes. Biochimica et Biophysica Acta (BBA) – Rev Biomembr 1998;1376:297–318.
45. Pham HT, Prendergast MB, Dunstan CW, Trevitt AJ, Mitchell TW, Julian RR, et al. Dissociation of proton-bound complexes reveals geometry and arrangement of double bonds in unsaturated lipids. Int J Mass Spectrom 2015;390:170–7.
46. Sato Y, Miyawaki O. Relationship between proton NMR relaxation time and viscosity of saccharide solutions. Food Sci Technol Res 2000;6:136–9.
47. Eikerling M. Transport phenomena in proton conducting media. J Phys Condens Matter 2011;23:230301.
48. Tewari KC, Kan N-S, Susco DM, Li NC. Viscosity, calorimetric, and proton magnetic resonance studies on coal liquid fractions in solution. Anal Chem 1979;51:182–5.
49. Bottomley PA. NMR imaging techniques and applications: a review. Rev Sci Instrum 1982;53:1319–37.
50. Espina R, Yu L, Wang J, Tong Z, Vashishtha S, Talaat R, et al. Nuclear magnetic resonance spectroscopy as a quantitative tool to determine the concentrations of biologically produced metabolites: implications in metabolites in safety testing. Chem Res Toxicol 2009;22:299–310.